Sol-gel processing of $R_xY_{3-x}Al_yFe_{5-y}O_{12}$ magneto-optical films

Masters of Science Thesis

by

Anders DiBiccari

Dr. Guo-Quan Lu, Dr. Sean Corcoran, Dr. William Reynolds

Virginia Polytechnic Institute and State University

Materials Science & Engineering Department

Blacksburg, Virginia

December 13, 2002

Keywords: sol-gel processing, rare earth and aluminum doped yttrium iron garnet, GGG, magneto-optical properties

Sol-gel processing of $R_xY_{3-x}Al_yFe_{5-y}O_{12}$ magneto-optical films

Anders DiBiccari

ABSTRACT

The goal of this research was the fabrication of thin films with magneto-optic (MO) properties. Accomplishment of this task was achieved via sol-gel processing of rare-earth and aluminum substituted yttrium-iron garnet ($R_xY_{3-x}Al_yFe_{5-y}O_{12}$, R,Al:YIG), where R= Bi, Gd, Er, Ho. Detailed are the processing conditions, parameters and results leading to R,Al:YIG films with MO response. Success was attained with a 0.25M Gd,Al:YIG solution spin coated for 120 seconds at 3500rpm onto a (111) gadolinium gallium garnet (GGG) substrate and calcinated at 900°C for 4 hours. Samples were characterized via x-ray diffraction (XRD), magneto-optical loop tracer, scanning electron microscopy (SEM), energy dispersive x-ray spectroscopy (EDS), profilometry and optical microscopy.

ACKNOWLEDGEMENTS

The author wishes to thank his advisor Dr. G.Q. Lu and committee members Dr. William Reynolds and Dr. Sean Corcoran. Additionally, Jess Calata for his brainstorming and recommendations, Sumitra Subrahaman for teaching the Rame Hart 100, Steve McCartney for the SEM/EDS results and David Gray for invaluable access to a Class 1000 clean room. Special thanks to Sean Christian and Dr. Paul Duncan of Airak, Inc. for their sponsorship of this work with an SBIR provided by DOE. Airak, Inc. is a small company located in Manassas, Virginia specializing in the development of harsh environment sensors.

TABLE OF CONTENTS

LIST OF MULTIMEDIA OBJECTS

CHAPTER 1 INTRODUCTION

1.1 Motivation and Outline

Industrial development has created growing demand for new types of sensors while physical environments have become tougher and more electromagnetically polluted. To overcome the pollution and realize other advantages, there has since the mid seventies, been a steadily growing interest in fiber optic sensors. Fiber optic remote sensing systems provide immunity to electromagnetic interference, electrical isolation and other advantages.[1]

The primary objective of the project was the development of a current sensor. The projected application of this material was a low cost, current sensor for power electronic systems. The aim of this thesis is the development of sol-gel processing techniques to produce a magneto-optical (MO) material suitable for high magnetic field sensing.

This thesis consists primarily of five parts: introduction, processing methodology, results and accomplishments, conclusions and recommendations for further study. A historical overview of magnetic sensors, prior YIG research, and sol-gel processing is provided. Sample preparation via sol-gel processing is covered in addition to processing conditions. The magneto-optical and other characterization tools utilized are detailed and enumerated. Characterization results and the progression of work performed are discussed. Finally, the significant successes and recommendations for future work are stated.

1.2 Background

Magnetic sensors have been used for navigation for well over 2,000 years. New technological applications need magnetic sensors with improved sensitivity, smaller size and compatibility with electronic systems. Today magnetic sensors can be used to reliably and accurately detect direction, presence, and rotation of magnetic fields and indirectly electric current. A number of magnetic sensors have been developed and can be easily classified by their magnetic field range, shown in Figure 1-1.[2]

Magnetic Sensor Technology	Detectable Field Range (gauss)*
	10^{-8} 10^{-4} 10^{0} 10^{4} 10^{8}
Squid	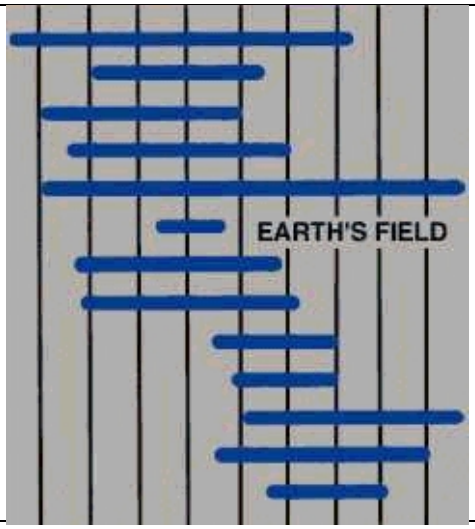
Fiber-Optic	
Optically Pumped	
Nuclear Procession	
Search-Coil	
Anisotropic	
Magnetorestrictive	
Flux-Gate	
Magnetotransistor	
Magnetodiode	
Magneto-Optical Sensor	
Giant Magnetoresistive	
Hall-Effect Sensor	

*1 Gauss = 10^{-4} Tesla = 10^{5} Gamma

Figure 1-1 Existing magnetic sensors and their detectable field ranges.

Every current has an associated magnetic field and vice versa. These are related by Maxwell's equations. Therefore any magnetic field sensing material has the potential to be utilized as a current sensor, provided application restrictions. A non-heat generating material with in-situ magnetic field sensing capability and is easily integrated in power electronic systems was the vision of this research.

A material with magneto-optical (MO) properties was identified as the most promising avenue to accomplish the vision shown in Figure 1-2. There are a number of magneto-optical materials, including flint glass (SF_6), BSO, BGO and garnets.[3] Garnets have more appeal due to their larger magnitude MO response. Substituted garnets, for example, show Faraday rotations in magnetic fields as low as 0.04 Tesla.[4]

Magnetic garnets have proven useful as MO devices because of their large Faraday rotations relative to other materials. Numerous studies involving magnetic garnets used as waveguides have inspired further exploration using rare earth iron garnets as possible media for next generation MO recording media.[5] Uses include electronic device sensors, magnetic bubbles used in logic operation, and memory elements for electronic computers. Extensive research with yttrium-iron garnet ($Y_3Fe_5O_{12}$, YIG) has established the material as the most common and well-known compound among rare

earth iron garnets. New MO effect devices including optical-communication components, gyrolasers and displays have implemented soft ferrite materials such as bismuth substituted yttrium-iron garnet ($Bi_xY_{3-x}Fe_5O_{12}$, Bi:YIG) or bismuth and aluminum substituted yttrium-iron garnet ($Bi_xY_{3-x}Al_yFe_{5-y}O_{12}$, Bi,Al:YIG).[6] The material chosen for the development of a MO film was substituted YIG. YIG has been used as an optical isolator in fiber optics and recently has been produced with rare earth and aluminum substitutions (R,Al:YIG), where R= Bi, Gd, Er, Ho, etc.[7] Faraday rotations of 50°/μm have been achieved with Bi,Al:YIG as compared with 12°/μm for YIG.[8] YIG has a complex cubic structure, shown in Figure 1-2. Note that iron occupies two different sites in the structure. The MO effect derives from the interaction of the iron atoms when exposed to a magnetic field. Bismuth or another rare earth element strengthens the effect by their diamagnetic properties.

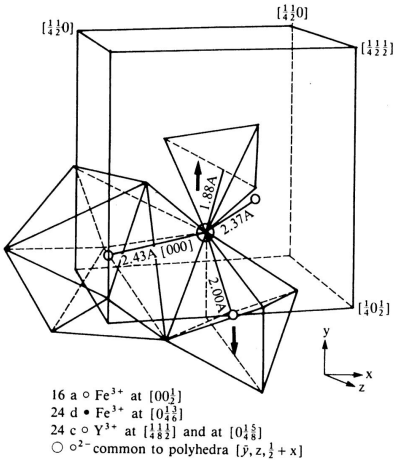

Figure 1-2 $Y_3Fe_5O_{12}$ crystal structure.[9]

A simplified depiction of the structure provides clarity into understanding the magnetization observed, shown in Figure 1-3. The ferrimagnetic garnets have the formula

$$\left(3M_2O_3\right)_c\left(2Fe_2O_3\right)_a\left(3Fe_2O_3\right)_d \quad \text{with} \quad \begin{matrix} 6Fe_d(30\mu_B)\uparrow \\ 4Fe_a(20\mu_B)\downarrow \\ 6M_c \quad \downarrow \end{matrix}$$

with M a trivalent rare-earth ion or yttrium ion. The subscripts show cation (a) is located in an octahedral site with 6 oxygen ions surrounding; (c) is a dodecahedral site surrounded with 8 oxygen ions; (d) surrounded with 4 oxygen ions forming a tetrahedral

site. A single cubic cell of ferrimagnetic garnet contains 160 atoms with a side being 8 molecules of $Fe_2Fe_3M_2O_{12}$, or approximately 12.4Å depending upon M. The magnetic moment arises from the antiparallel coupling between (a) and (d) ions with the (c) ion oriented antiparallel to the (d) ion. The net moment, m_s, in Bohr magnetons per unit formula $3M_2O_3 \cdot 5Fe_2O_3$ is

$m_s = 6\ m_c - (6\ m_d - 4\ m_a) = 6\ m_c - 10\ \mu_B$.

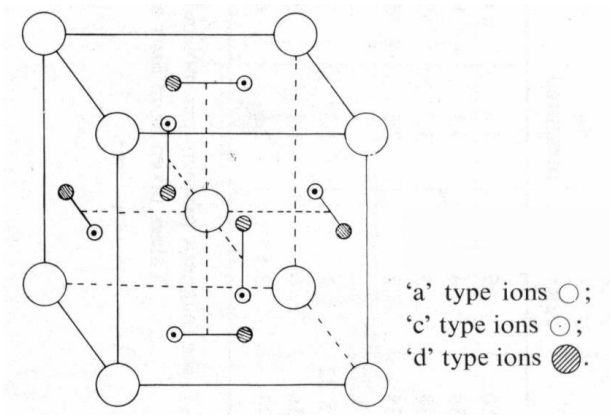

Figure 1-3 Simplified garnet structure of unit $(Fe_2)_a\ (Fe_3)_d\ (M_2)_cO_{12}$.

Currently varieties of applications and processes have been implemented for YIG film production via liquid phase epitaxy (LPE), sol-gel, reactive ion beam sputtering, and chemical vapor deposition (CVD).[10,11] Sol-gel was the proposed process for film production due to advantages including low synthesis temperature and low cost. It is a wet chemical approach where solid precursors are dissolved into a solvent. As shown in Figure 1-4 sol-gel solutions can be formed into thin films, aerogels, powders, etc.

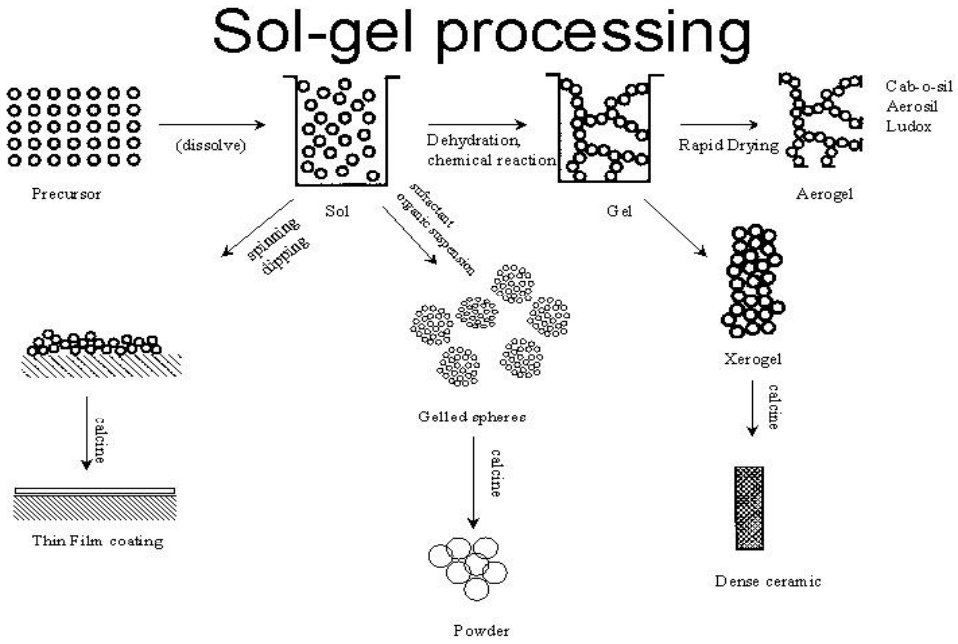

Figure 1-4 Sol-gel processing methodology.[12]

CHAPTER 2 EXPERIMENTAL

2.1 Pre-processing

Materials

Nitrates, sulphates, chlorides, alkoxides, and acetates are all viable sources to produce a multicomponent gel. Alkoxides are often not cost effective compared with other precursors. Acetates are more soluble than nitrates but do not thermally degrade as well. Nitrates do thermally degrade, do not have as strong covalent bonding to the anion, and are low cost. They do have the drawback of being highly oxidizing and therefore difficulties in controlling reaction chemistry can arise.[13] The materials to prepare $Bi_xY_{3-x}Al_yFe_{5-y}O_{12}$ were the same as referenced in the literature. All sol-gel solution precursor materials were obtained from Alfa Aesar. Hydrated forms of iron nitrate, yttrium nitrate, aluminum nitrate and bismuth nitrate were the metal solutes. Purity of the hydrated metal nitrates was 98.5% or higher. The solvents used were ethylene glycol and ethyl aceto acetate with 99.9% purity. Nitric acid at 60% by volume and propionic acid was also used.

Substrate materials included: alumina, microscope (glass) slides, quartz, (110) silicon, and (111) gadolinium gallium garnet (GGG). GGG was purchased from MTI Corporation and Mol-Tech, Gmbh. Silicon wafers were used as the primary substrate due to widespread industrial application and monetary considerations.

2.2 Sample Preparation

Processing includes sol-gel formulation methodology, deposition techniques and calcination profiles. The sol-gel formulation methodology describes the progression of mixing procedures, dopants and solvent systems utilized. Deposition techniques included spin coating, dip coating, and a modified casting process. Progression of calcination profiles is detailed with a pictorial of the sol-gel formulation/calcination profile experiments performed.

2.2.1 Mixing Procedures

Bismuth and aluminum doping of the base material, yttrium iron oxide, was prepared via the sol-gel method. Targeted chemical formulas included $Bi_{3-x}Y_xAl_yFe_{5-y}O_{12}$, with x=0.5 and 1 and y=0.2 and 0.4. Processing techniques whereby hydrated metal nitrates were hydrolyzed with ethylene glycol and nitric acid to obtain a sol-gel solution with the above targeted molecular formulas were utilized.[3,4]

Solutions were prepared by dissolving $Fe(NO_3)_3$, $Al(NO_3)_3$, and $Y(NO_3)_3$ in ethylene glycol and $Bi(NO_3)_3$ in nitric acid, combining the two mixtures and heating in a nitrogen atmosphere. For example, to prepare a 25mL, 0.125 molar solution with molecular formula $Bi_2Y_1Fe_{4.6}Al_{0.4}O_{12}$, 5.2828g $Fe(NO_3)_3$, 0.4800g $Al(NO_3)_3$, and 1.1969g $Y(NO_3)_3$ were dissolved in 23mL of ethylene glycol and 3.1173g $Bi(NO_3)_3$ in 2mL of nitric acid. To completely dissolve the $Bi(NO_3)_3$ in nitric acid, heating approximately 10 minutes at 50±2°C was required. The two mixtures were combined and heated in a water bath at 80 ± 2°C in a nitrogen atmosphere for 50 minutes. Shown in Figure 2-1 is the experimental setup utilized to heat the solution while under a nitrogen atmosphere. Alternative mixing procedures developed are discussed in Section 3.2.

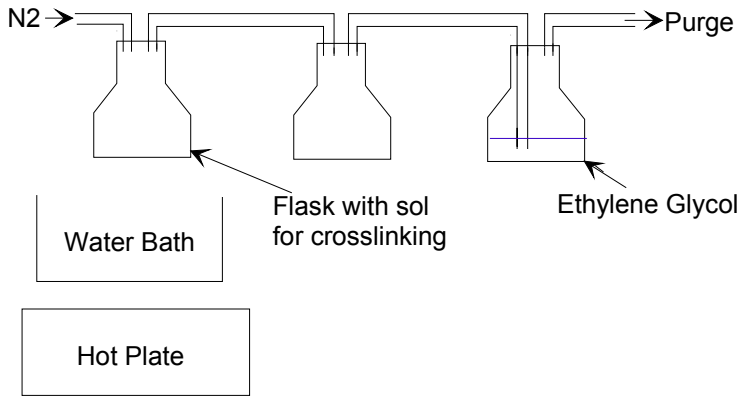

Figure 2-1 Experimental setup for heating sol-gel formulations.

Table 2-1 lists Bi,Al:YIG mixtures in ethylene glycol prepared with the associated molecular formulas, concentrations, and heating times. Various concentrations were attempted ranging from 0.042 to 0.5 molar. The ID column in Table 2-1, Table 2-2 and Table 2-3 indicates the principal solvent used by the abbreviation, i.e. EG is ethylene glycol, EAA is ethyl aceto acetate.

Table 2-1 Bi,Al:YIG formulations in ethylene glycol.

Mixture ID	Molecular Formula	Concentration (Mol/L)	Heating Time (min)
EG-1	$Bi_{2.5}Y_{0.5}Fe_{4.2}Al_{0.8}O_{12}$	0.042	150
EG-2	$Bi_{2.5}Y_{0.5}Fe_{4.2}Al_{0.8}O_{12}$	0.40	30
EG-3	$Bi_{2.5}Y_{0.5}Fe_{4.2}Al_{0.8}O_{12}$	0.125	50
EG-4	$Bi_{2.5}Y_{0.5}Fe_{4.2}Al_{0.8}O_{12}$	0.15	60
EG-5	$Bi_{2.5}Y_{0.5}Fe_{4.2}Al_{0.8}O_{12}$	0.50	20
EG-6	$Bi_2Y_1Fe_{4.6}Al_{0.4}O_{12}$	0.50	20
EG-7	$Bi_2Y_1Fe_{4.6}Al_{0.4}O_{12}$	0.25	35

Alternative formulations pursued with different solvent systems, ethylene glycol and ethyl aceto acetate, are shown in Table 2-2. Table 2-3 lists stock solution methodology formulations (discussed in Section 3.2) with associated molecular formula, solution concentration and solvents. Note SS indicates stock solution methodology and all formulations using ethylene glycol and ethyl aceto acetate were a 50/50 solvent ratio.

Table 2-2 Alternative solvent system formulations.

Mixture ID	Molecular Formula	Concentration (Mol/L)
EAA-1	$Bi_2Y_1Fe_{4.6}Al_{0.4}O_{12}$	0.25
EG/EAA-1	$Bi_2Y_1Fe_{4.6}Al_{0.4}O_{12}$	0.50
EG/EAA-2	$Bi_2Y_1Fe_{4.6}Al_{0.4}O_{12}$	0.25
EG/EAA-3	$Bi_2Y_1Fe_{4.6}Al_{0.4}O_{12}$	0.125
EG/EAA-4	$Y_3Fe_5O_{12}$	0.25

Table 2-3 Formulations via stock solution with solvents utilized.

Mixture ID	Molecular Formula	Concentration (Mol/L)	Solvents
SS-1	$Bi_2Y_1Fe_{4.6}Al_{0.4}O_{12}$	0.25	EG
SS-2	$Bi_2Y_1Fe_{4.6}Al_{0.4}O_{12}$	0.25	EG/EAA
SS-3	$Dy_2Y_1Fe_{4.6}Al_{0.4}O_{12}$	0.25	EG/EAA
SS-4	$Er_2Y_1Fe_{4.6}Al_{0.4}O_{12}$	0.25	EG/EAA
SS-5	$Gd_2Y_1Fe_{4.6}Al_{0.4}O_{12}$	0.25	EG/EAA

2.2.2 Deposition Techniques

Thin film deposition via dip and spin coating techniques on alumina, microscope (glass) slides, quartz, (110) silicon, and (111) GGG substrates was conducted. Casting of thick films on (110) silicon and (111) GGG was also accomplished. Procedures for each

of the deposition techniques are summarized below. Several substrate pretreatment techniques were investigated for improved film wetting characteristics.

Substrate Pretreatment

Substrates of 1”x1” glass slides, 1”x1” quartz, 1”x1”, ½”x½”, and ¼”x¼” (110) Si, and ½”x½” and ¼”x¼” GGG crystals were used for depositing the sol-gel derived Bi,Al:YIG and R,Al:YIG. Initially, deposition of the derived sol-gel liquids was done on silicon wafers obtained directly from the manufacturer’s packaging. To ascertain wetting characteristics and improve film adhesion various substrate pretreatment techniques were evaluated. Table 2-4 lists the various pretreatment techniques employed. As shown, the pretreatment techniques ranged from a simple acetone rinse to plasma cleaning in an Argon atmosphere and are detailed below:

Technique 1: Silicon substrate placed in an ultrasonic cleaner approximately 10 minutes using acetone followed by a rinse with deionized water and spin dried.

Technique 2: Acetone was sprayed on silicon wafers followed by scrubbing using lint-free Kimwipes.

Technique 3: Acetone was sprayed on silicon wafers followed by scrubbing using lint-free Kimwipes and a deionized water rinse.

Technique 4: Ethanol was sprayed on the silicon wafer followed by scrubbing using lint-free Kimwipes.

Technique 5: Ethanol cleaning followed by a 25% by volume hydrofluoric acid dip and scrubbing with a Kimwipe using ethyl alcohol.

Technique 6: Ethanol cleaning followed by a 25% by volume hydrofluoric acid dip and scrubbing with a Kimwipe using deionized water.

Technique 7: Ultrasonic cleaning of silicon substrates with a 60% by volume nitric acid bath for 10 minutes followed by a 10 minute ultrasonic bath of acetone, a deionized water rinse and spin dried.

Technique 8: 10 minutes of ultrasonic cleaning in a 25% by volume hydrofluoric acid bath followed by another 10 minutes of ultrasonic cleaning in an acetone bath, a deionized water rinse and spin dried.

Technique 9: A 45% by weight potassium hydroxide (KOH) solution was used to clean silicon substrates by dipping and spin dried.

Technique 10: Silicon wafers were placed in an Argon plasma cleaner from 1 to 5 minutes.

All of the techniques were performed in both a modular clean room and a laboratory environment. Technique 4 was also performed in a Class 1000 clean room environment on both (110) silicon and (111) GGG wafers.

Table 2-4 Substrate surface pretreatments.

Technique	Si (110)	GGG (111)	Al_2O_3	Quartz	Glass Slide
No treatment	X	X	X	X	X
1	X				
2	X	X	X	X	X
3	X				
4	X	X	X	X	X
5	X				
6	X				
7	X				
8	X				
9	X				
10	X				

Spin coating

Deposition of sol-gel derived solutions was accomplished via spin coating. Preliminary spin coating was performed using silicon wafers leading to GGG substrate. Substrate geometry included circular 4 diameter wafers as well as diced wafers of 1”x1”, ½”x½” and ¼”x¼” dimensions. Spin coating was conducted in a laboratory environment, modular and class 1000 clean room.

The spin coating process included two steps: 1) spin-on and 2) spin-off. The spin-on step employed a low spin rate (500-2000 rpm) with a variety of cycle times (10-120 seconds). During this step the sol-gel solution was deposited on the substrate and allowed to spread. The spin-off step employed high spin rates (2000-6000rpm) with a constant cycle time of 120 seconds. A higher spin rate was used for the spin-off step for removal of excess liquid and determination of final film thickness. A wide range of spin

rates and times were investigated to determine optimal processing parameters for the sol-gel derived films. Spin-on rates attempted included 500, 1000, and 1500 rpm with cycle times of 10, 30, 45, 60, 90 and 120 seconds. Spin-off rates 2000, 2500, 3000, 3500, 4000, 4500, 5000, 5500, and 6000 rpm were investigated with each of the spin-on iterations.

Dip coating

A simple dip coater was fabricated based on literature references. The technique encompassed taping a substrate to a string attached to a floating object with mass greater than the substrate, the schematic is shown in Figure 2-2. Substrate removal rate from the sol-gel reservoir was controlled by the flow of water released from the holding tank.

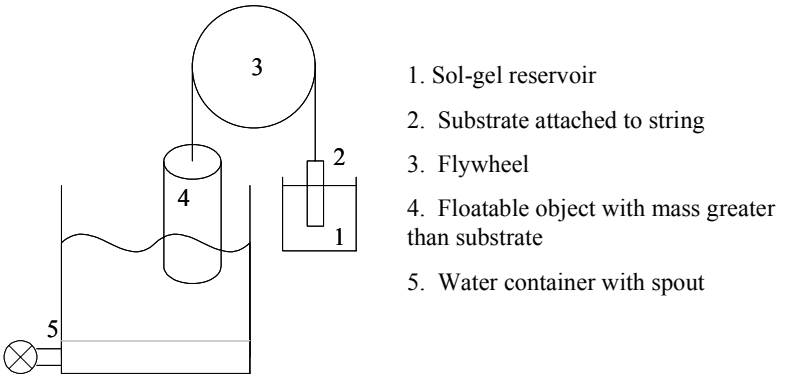

Figure 2-2 Schematic of developed dip coater.

Dip coating was performed only with 1"x1" and ½"x½" (110) silicon and ¼"x¼" (111) GGG wafers. Dip coating rates of 1, 1.5, 2 and 2.5cm/min (the rate limitation of available equipment) were evaluated. Dip coating was performed solely in a laboratory environment.

Casting

The final deposition methodology utilized was a simple technique based on casting technology. Substrates used were 1"x1", ½"x½", and ¼"x¼" (110) silicon and ½"x½", and ¼"x¼" (111) GGG. This technique included pipetting an excess of sol-gel solution onto the substrate, allowing the liquid to completely wet the surface for 30 seconds, followed by removal of the liquid by a gravitational technique. Removal of the liquid

was accomplished by placing the substrate on a Kimwipe and tilting the substrate to approximately 75° to allow the excess liquid to drain off. Casting was performed solely in a laboratory environment.

2.3 Processing Conditions

Heating a sol-gel solution to form a crystalline material is the act of calcination. Sol-gel liquid films were exposed to various calcination profiles in attempts to form garnet crystal. A Fisher Scientific IsoTemp and a Lindberg/Blue quartz tube furnace were used to calcine films. Calcination profiles were performed in a laboratory environment except where noted. The identification for the calcination profiles is based upon the steady state temperatures and denoted as CP-1 through CP-17. A typical calcination profile is shown in Figure 2-3.

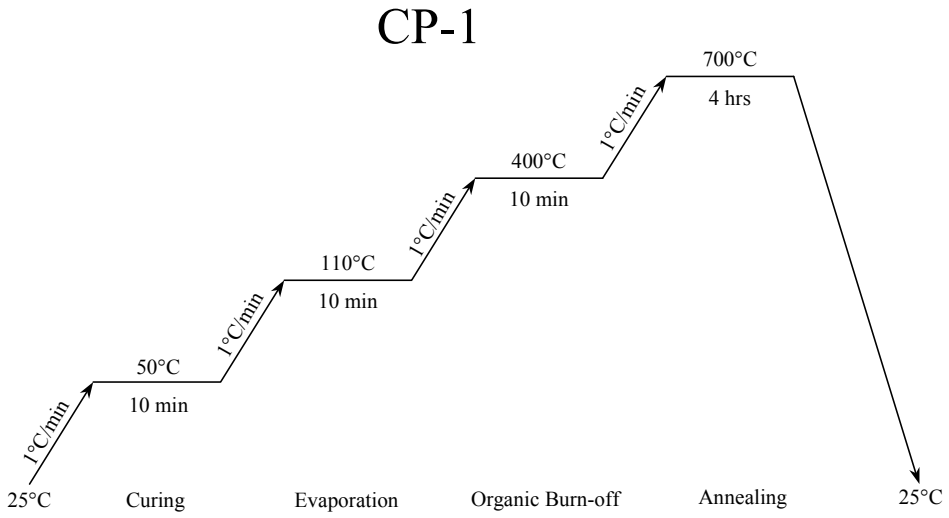

Figure 2-3 Typical calcination profile.

2.4 Characterization methods

A variety of material characterization techniques were utilized at various stages of film processing. Optical microscopy, X-ray diffraction (XRD) and a MO loop tracer were used to determine film quality, structure and MO response, respectively. Ellipsometry and surface profilometry were used to determine film thickness. Scanning electron microscopy and energy dispersive x-ray spectroscopy (SEM/EDS) was used to characterize surface morphology and elemental composition. Contact angle

measurements were used to ascertain the effects of the various substrate pretreatment techniques with respect to film wettability and adhesion.

Magneto-Optical Loop Tracer

The MO loop tracer is widely utilized to measure MO response of materials.[14] Geometric optics was used to identify and quantify the physical property known as the Faraday rotation. The Faraday rotation is defined by:

$$F = BVl$$

Where B is the magnetic field, V the Verdet constant and l is the sample length. A Faraday rotation is the rotation of linearly polarized light from an initial state to some angle, φ, as the light propagates through a sample medium with a parallel applied magnetic field. The magnetic field affects the interactions of localized magnetic moments inducing the rotation of the light. Two orthogonal detectors were placed in the laser beam path after passing through a sample. A sample was then placed in a magnetic field oriented parallel with the laser beam causing the rotation of polarized light, which affects the intensity of the light entering each detector. Geometric optics states that rotation of light will be accompanied by an increase in signal intensity in one detector and a decrease of intensity in the orthogonal detector. A schematic of the MO loop tracer is shown in Figure 2-4. Given the thickness of the film and magnitude change in the signal, a Faraday rotation can be determined. Films on both reflective and transparent substrates can be interrogated via the MO loop tracer due to the ability to reflect the laser beam off the substrate or the substrate placed on a mirror, respectively.

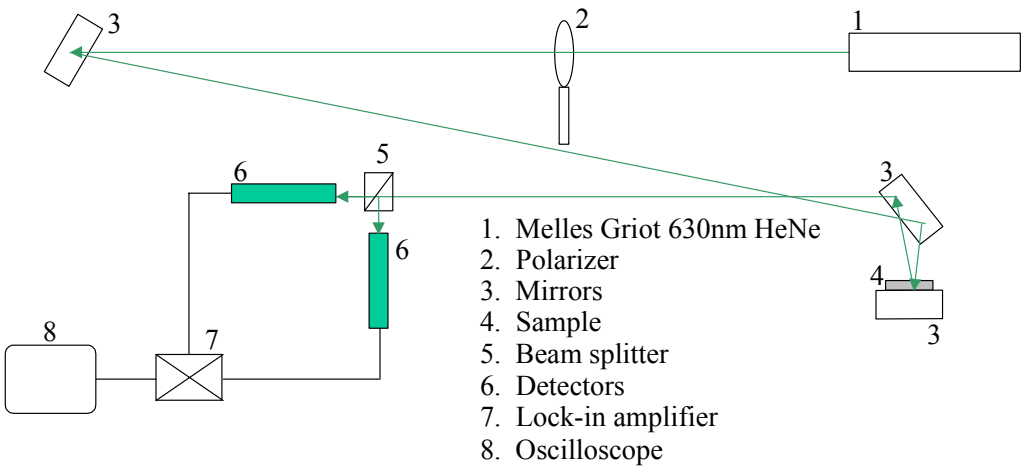

Figure 2-4 Magneto-optical loop tracer schematic.

A 630nm Helium-Neon laser (Melles Griot) enters the sample perpendicular to the sample surface, reflects off a mirror and through the sample a second time before being split into two orthogonal detectors. The laser passed through a linear polarizer prior to entering the sample. To determine MO response, the sample was placed in a magnetic field orthogonal to the laser beam. This was accomplished by sliding a solid-state magnet under the sample while subjected to the laser. Strength of the permanent magnet was approximately 270mT. Airak, Inc provided the MO loop tracer shown in Figure 2-5.

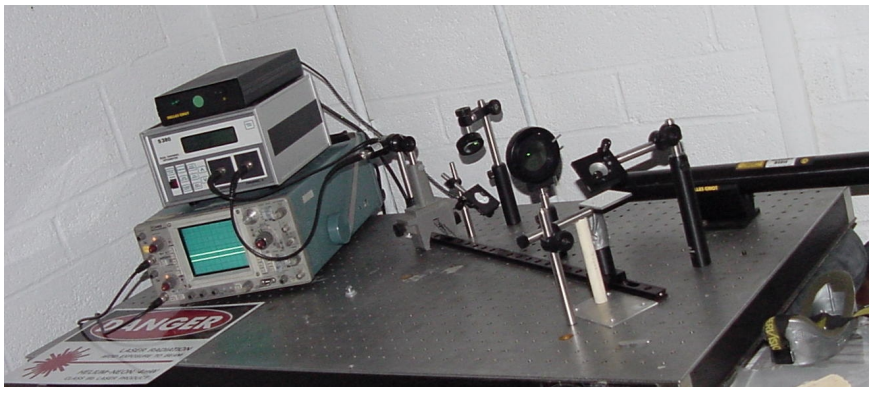

Figure 2-5 Magneto-optical loop tracer.

X-ray Diffraction

Diffraction patterns associated with the Bi,Al:YIG structure from literature, shown in Figure 2-6, were used as a reference for sol-gel derived samples. In addition, the JCPDS powder diffraction database was used to compare diffraction patterns for Bi,Al:YIG.

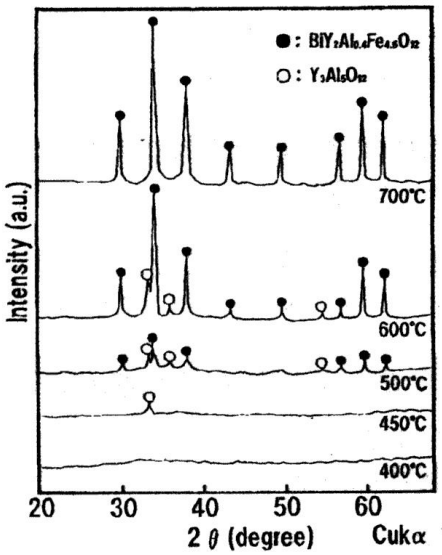

Figure 2-6 XRD of Bi,Al:YIG powder as a function of temperature.[2]

X-ray diffraction studies were conducted on a Scintag XDS 2000 powder diffractometer courtesy of the Geology Department. The wavelength of X-ray radiation used was from a copper source with $K_{\alpha 1}$ = 1.5405Å, $K_{\alpha 2}$ = 1.5443Å, K_{β} = 1.3922Å. Films and powders were investigated and compared with literature data. Diffractometer sample holders were solid steel with a 1 cm^3 capacity. Sample preparation was similar for films and powders. Films were either placed or taped in the sample holder. Processed powders were ground using a mortar and pestle and placed on a quartz plate with ethyl alcohol then placed in the steel sample holder. A 2θ range of 6-120° was initially used. Further experiments reduced the range to 10-90°. A scan rate of 0.5°/min was used for all runs. All samples were rotated while scanned.

Surface Profilometry

Ellipsometry, an optical characterization method, was utilized to determine optical properties of materials including absorption coefficients, refractive indices and reflectivity. The technique is based on the principles of reflection of polarized light. It measures the ratio of Ψ and Δ (the amplitude and phase components of polarized light, respectively) thereby requiring no reference material and providing highly accurate and reproducible characterization. The presence of very thin films can accurately be resolved down to the sub-angstrom scale. Multiple industries and academics employ the technique for metrology.

A variable angle spectroscopic ellipsometer (VASE) was used for determining film thickness on silicon and GGG. The ability to measure film thickness on a variety of different substrates, especially GGG, was of importance. The optical constants and film thickness were calculated with the Lorentz model. Sample preparation was important for ellipsometry because a vacuum was used to hold samples in place. Any sample smaller than ½"x½" required another substrate with dimensions greater than a ½"x½".

Profilometry is a mechanical characterization tool that uses line-scan geometry for measuring surface topography. It is useful in identifying surface texture, step heights, widths, spacing and radius of curvature. A diamond tipped stylus is moved along a sample surface with surface features translated directly into a viewable map of the film variations. Unlike ellipsometry, profilometry requires no mathematical manipulation to determine surface characteristics.

A Dektak3 was used to measure film thickness. The technique required a portion of the substrate to be free of film to provide a reference. Samples were placed on the stage and oriented such that the stylus was approximately 100μm from the film. Limitations of this approach were due to the maximum measurement length of 1mm per run.

SEM/EDS

SEM is a well-established technique used for surface morphology characterization and qualitative elemental analysis. SEM exposes a sample under vacuum to a collimated electron beam. The sample emits both secondary electrons and x-rays in response to this

energy. SEM imaging is attained by collecting secondary electrons emitted by the sample.

EDS utilizes the x-rays emitted by a sample to perform chemical microanalysis. Qualitative determination of elements present is obtained by analyzing a spectrum of the number of emitted x-rays versus their energy. EDS provides elemental composition of features and phases as small as ~ 1μm. SEM and EDS can be performed simultaneously because two different energy sources are collected and measured from the sample, secondary electrons and x-rays, respectively.

Both low and high-temperature films with MO response were examined with SEM/EDS. Samples were coated with gold to eliminate the sample charging. Steve McCartney performed all sample analysis.

Optical Microscopy

Film characteristics such as thickness uniformity and cracking were examined by optical microscopy. Attributes were examined with an Olympus BH-2 microscope under magnifications of 5x, 10x, 20x, 50x, and 100x and recorded using an MTI CCD72S digital camera. Sample preparation was not critical; any section of a film surface on a substrate up to 4" in diameter was viewable. Even films that were nearly transparent on glass slides, quartz and GGG were viewable, especially when films were non-uniform. The following technique was used to examine thin films:

- focus on the edge of the substrate;
- move stage to the center of the substrate to focus on the film surface as opposed to the bulk substrate.

Contact Angle Measurement

The surface tension of a solid/liquid system can be determined via contact angle measurements. In addition, contact angle measurements can be used to assess the hydrophilicity/hydrophobicity of a solid surface. Knowledge of a surface's general nature eliminates experiments with countless liquids. Contact angle measurements have been correlated with surface properties of tension over the past four decades. The contact angle of a sessile or pendant drop of liquid resting on a solid provides the surface tension

of the liquid/solid system. A Ramehart contact angle goniometer was used to collect contact angles, a typical setup is shown in Figure 2-7.

Figure 2-7 Ramehart contact angle goniometer.

Four substrate pretreatment techniques on (110) silicon were evaluated with respect to no substrate pretreatment using a Ramehart 100 contact angle goniometer. Substrate pretreatment techniques #3, 4, 6 and 7 (see Table 2-4) were evaluated and compared with unmodified (110) silicon by measuring the contact angle of methylene iodide and distilled water on the substrates. Approximately 5μL of each liquid was placed on the surface of each sample and the contact angle was measured. This process was repeated a minimum of 7 times per liquid per sample to ensure validity of measurements.

CHAPTER 3 Results and Discussion

3.1 Mixture Iterations

Chemistry was of utmost importance to develop a sol-gel derived material. The ability to prepare sol-gel solutions with expected concentrations was key to developing magneto-optic films. Due to alterations in the mixing procedures three iterations of mixing calculations were used. All calculations were based on the general formulation:

$$M_xV_x=M_yV_y \qquad \text{Eq. 3.1}$$

where M_x is the molarity and V_x is the volume of component x. The system contained four key constituents, elements Fe, Y, Bi, and Al. Literature references the optimum molecular formula was $Bi_{3-x}Y_xAl_yFe_{5-y}O_{12}$ with x=0.5 and y=0.2.[9,10]

Each metal nitrate was hydrated with varying amounts of water. Determination of each metal nitrate mass was based on a targeted volume and molar concentration allowing for the mass due to hydration. Iteration #1, shown in Figure 3-1, incorporated the components stated above. Unfortunately an error in calculation occurred and the $Al(NO_3)_3$ added was almost five times the required amount. An alternative mixing approach using stock solutions, Section 3.2, required new mixture calculations termed Iteration #2 and displayed in Figure 3-2. Shown are the masses of each hydrated metal nitrate calculated for 100mL stock solutions at 0.46, 0.4, 2, and 1M for $Fe(NO_3)_3$, $Al(NO_3)_3$, $Y(NO_3)_3$, and $Bi(NO_3)_3$, respectively. The volume of each stock solution needed to prepare a 50mL, 1.27M solution of $Bi_2Y_1Fe_{4.6}Al_{0.4}O_{12}$ is also shown. Iteration #2 was not versatile to changing final molar concentrations using mixed stock solutions. Therefore Iteration #3 was developed, shown in Figure 3-3, it combined Iterations #1 & 2 and simplified stock solution calculations. By merely changing the molarity of the solution in Iteration #3 the new volumes of each stock solution needed are given. Figure 3-1 Original mixing procedure, Iteration #1. and Figure 3-3 represent the mass of metal nitrates and solvent volume required to prepare a 0.125M, 25mL solution of $Bi_2Y_1Fe_{4.6}Al_{0.4}O_{12}$.

Primary Input	Primary Input
Molarity of **s**olution ***Ms*** (mol/L)	**V**olume of **s**olution ***Vs*** (mL)
0.125	25

Primary Input	
Element	Comp of YIG
Y	1
Fe	4.6
Bi	2
Al	0.4

weight of each hydrated crystal needed			
Y (g)	Fe (g)	Bi (g)	w(Al)
1.1969	5.2818	3.1173	2.3998

Figure 3-1 Original mixing procedure, Iteration #1.

Ratiometric Scalar	0.1
Add Solvent to Each	0.05 (L)

Molecular Weights (g/mol)

g/mol (Y)	g/mol (Fe)	g/mol (Bi)	g/mol (Al)
383.01	403.99	394.99	375.13

Number of Mols

n(Y)	n(Fe)	n(Bi)	n(Al)
0.1	0.46	0.2	0.04

Weight (g)

g (Y)	g (Fe)	g (Bi)	g (Al)
38.301	185.8354	78.998	15.0052

Molarity of Solns (mol/L)

M (Y)	M (Fe)	M (Bi)	M (Al)
2	9.2	4	0.8

Estimated YIG Molecular Weight (g/mol)
966.6454

Stock Volume (L) 0.01 (L)

	Vol (L)	Molarity (Mol/L)	Mols	Weight (g)	Molarity of Final Soln (mol/L)
Fe	0.01	9.2	0.092	35.23692	1.272066
Y	0.01	2	0.02	8.0798	
Al	0.01	0.8	0.008	3.15992	
Bi	0.01	4	0.04	15.0052	
Dilution Volume	0.01				

Figure 3-2 Stock solution mixture calculations, Iteration #2.

To make single solution:

Primary Input	Primary Input									
Molarity of **s**oln	Total **V**ol of **s**oln	# moles of yig	# mols of each element				wt of each hydrated crystal needed			
Ms (mol/L)	***Vs*** (mL)	n(YIG)	n(Y)	n(Fe)	n(Bi)	n(Al)	w(Y)	w(Fe)	w(Bi)	w(Al)
0.125	25	0.003125	0.003125	0.014375	0.00625	0.00125	1.1969	5.2818	3.1173	0.4800

Primary Input	
Element	Comp of YIG
Y	1
Fe	4.6
Bi	2
Al	0.4

To make stock solutions at *x* M concentrations:

Input	Input								
Stock solution vol	Target Molarity **(xM)**	# mols of each element				wt of each hydrated crystal needed			
		n(Y)	n(Fe)	n(Bi)	n(Al)	w(Y)	w(Fe)	w(Bi)	w(Al)
50	2.3	0.115	0.115	0.115	0.115	44.0473	42.2545	57.3586	44.1566

Amount of stock solutions needed to make *Ms* & Vs single solution:

			Calc check: if Ms and Vs are same as above, g and mols same too	
	Vol (mL)	Molarity	g	mols
Fe	6.25	2.3	5.2818	0.014375
Y	1.36	2.3	1.1969	0.003125
Al	0.54	2.3	0.4800	0.00125
Bi	2.72	2.3	3.1173	0.00625
Total Vol. Stock solns added	10.87			
Solvent needed to satisfy **Vs**	14.13			

Figure 3-3 Combination of stock solution and original mixing calculations, Iteration #3.

3.2 Processing & Characterization

3.2.1 Formulations

The sol-gel formulations developed are shown in Table 3-1. Each was examined with respect to processing time and film quality while altering solution concentration, dopants, heating times and solvents. Formulations associated with films displaying MO response and powders with garnet crystal structure are highlighted in red and blue, respectively. As can be seen only 0.25M solutions provided garnet crystal structure or MO response. Development of this table via mixing procedure changes is described below.

Molarity was the first parameter varied with heating times being a dependent variable of the concentration. Solutions attempted included 0.042, 0.125, 0.15, 0.25, 0.4 and 0.5M. Solution concentrations of 0.25M were deemed most appropriate with respect to processing time. No sol-gel reaction was observed with a 0.042M solution after 150 minutes of heating at 80°C in an N_2 atmosphere and was therefore discarded. Molar concentrations exceeding 0.25M required 15-60 minutes of sonic agitation to fully

dissolve the nitrate salts into ethylene glycol at 25°C. Additionally, sol-gel chemistry often led to uncontrolled exothermic reactions with solution concentrations above 0.4M. The strength of the explosive reactions was unexpected as no journal article using sol-gel chemistry of nitrates mentioned inability to control sol-gel reactions. Reference topics of nitrate chemistry stated decomposition of nitrates may be controlled, but high activation energy leads easily to explosive reaction.[15] Therefore alterations in the original mixing procedure were implemented and include:

1. Dehydration of the nitrate crystals;
2. Storage of bulk solutions at 5°C;
3. $Bi(NO_3)_3$ dissolved in ethylene glycol and adding nitric acid to the total solution while in a water bath at 80 ± 2°C in a nitrogen atmosphere;
4. removal of nitric acid from the solution.;
5. heating in a 80 ± 2°C water bath in ambient atmosphere;
6. removal of the heated water bath;
7. ethyl aceto acetate as an alternative solvent;
8. stock solutions (separate solutions for each metal nitrate);
9. simplification of the procedure/chemistry by removal of bismuth and aluminum dopants;
10. alternative rare-earth elements as dopants;

Of these changes, only numbers five and six were successful in eradicating uncontrolled exothermic reactions. All of the modified mixing procedures are described below.

Table 3-1. Sol-gel solution formulations

Mixture ID	Molecular Formula	Concentration (mol/L)	Heating Time (min)	Solvent(s)
EG-1	$Bi_{2.5}Y_{0.5}Al_{0.8}Fe_{4.2}O_{12}$	0.042	150	EG
EG-2	$Bi_{2.5}Y_{0.5}Al_{0.8}Fe_{4.2}O_{12}$	0.4	30	EG
EG-3	$Bi_{2.5}Y_{0.5}Al_{0.8}Fe_{4.2}O_{12}$	0.125	50	EG
EG-4	$Bi_{2.5}Y_{0.5}Al_{0.8}Fe_{4.2}O_{12}$	0.15	60	EG
EG-5	$Bi_{2.5}Y_{0.5}Al_{0.8}Fe_{4.2}O_{12}$	0.5	20	EG
EG-6	$Bi_2Y_1Al_{0.4}Fe_{4.6}O_{12}$	0.5	20	EG
EG-7	**$Bi_2Y_1Al_{0.4}Fe_{4.6}O_{12}$**	**0.25**	**35**	**EG**
EAA-1	$Bi_2Y_1Al_{0.4}Fe_{4.6}O_{12}$	0.25	N/A	EAA
EG/EAA-1	$Bi_2Y_1Al_{0.4}Fe_{4.6}O_{12}$	0.50	N/A	EG/EAA
EG/EAA-2	$Bi_2Y_1Al_{0.4}Fe_{4.6}O_{12}$	0.25	N/A	EG/EAA
EG/EAA-3	$Bi_2Y_1Al_{0.4}Fe_{4.6}O_{12}$	0.125	N/A	EG/EAA
EG/EAA-4	***$Y_3Fe_5O_{12}$***	***0.25***	***N/A***	***EG/EAA***
SS-1	$Bi_2Y_1Al_{0.4}Fe_{4.6}O_{12}$	0.25	N/A	EG/EAA
SS-2	$Bi_2Y_1Al_{0.4}Fe_{4.6}O_{12}$	0.25	N/A	EG/EAA
SS-3	$Dy_2Y_1Al_{0.4}Fe_{4.6}O_{12}$	0.25	N/A	EG/EAA
SS-4	$Er_2Y_1Al_{0.4}Fe_{4.6}O_{12}$	0.25	N/A	EG/EAA
SS-5	**$Gd_2Y_1Al_{0.4}Fe_{4.6}O_{12}$**	**0.25**	**N/A**	**EG/EAA**

Discovery of the highly exothermic nature of the solution prompted two methods to prevent further uncontrolled reactions: 1) dehydration of the nitrate crystals and 2) storing solutions at 5°C. Metal nitrates were dehydrated at 135°C in a Fisher furnace. Complete dehydration was gravimetrically determined using an Ohaus balance; time of dehydration ranged from 140 minutes for $Al(NO_3)_3$ to 270 minutes for $Fe(NO_3)_3$. All solutions were stored at 5°C to reduce the overall reaction kinetics and thus uncontrolled reactions. Bubbling and pressure increase was observed in refrigerated solutions above 0.4M.

Nitric acid was believed to be a reaction promoter by providing protons; therefore experiments to eliminate uncontrolled reactions included delaying addition of nitric acid and removing it completely from the system. Neither approach prevented uncontrolled reactions. Literature discussed sol-gel processing of YIG in both nitrogen and ambient atmospheres; therefore heating in ambient atmosphere was attempted maintaining all other procedures detailed in Section 2.2.1. Uncontrolled reactions were not abated by the above methods and heating in an ambient atmosphere actually aggravated the situation, as there was no cooling capability to slow or stop the reaction. Observation of the solution following nitrate salt dissolution revealed a viscosity appropriate for spin

coating, therefore removing the heating bath step was implemented to eliminate the chance of an exothermic reaction. Solutions not heated were observed to bubble while stored at 5°C.

Ethyl aceto acetate was referenced as an alternative solvent in preparing Bi,Al:YIG and was subsequently used as a replacement for ethylene glycol.[2,6] Metal nitrates required additional time (15-45 min) to dissolve in ethyl aceto acetate. Solutions using only ethyl aceto acetate did not exhibit uncontrollable reactions, however $Fe(NO_3)_3$ would not fully dissolve when solution concentrations were above 0.4M. It was believed that individual solutions of each nitrate separately dissolved in ethylene glycol or ethyl aceto acetate would eradicate the continued reactions. This led to the introduction of stock solution methodology and mixing Iteration#2. Reduction in time of processing would also be realized by removing the time to dissolve the nitrate salts each time a new solution was needed. The $Fe(NO_3)_3$ was determined to be the cause of the exothermic reactions. A 50/50 ratio of ethyl aceto acetate and ethylene glycol in stock solution methodology was subsequently introduced in addition to dissolution of the $Fe(NO_3)_3$ a few minutes prior to sol-gel formation as compared with $Al(NO_3)_3$, $Y(NO_3)_3$, and $Bi(NO_3)_3$ nitrates which were mixed hours or days in advance. Combination of these two safety steps significantly reduced risks of an uncontrolled reaction during the mixing step.

Simplification and verification of the mixing process was implemented by combining only $Fe(NO_3)_3$ and $Y(NO_3)_3$ to produce yttrium iron garnet (YIG). To produce the material at 0.25M with the desired $Y_3Fe_5O_{12}$ formula mixing calculation Iteration #3, Figure 3-3, was used to calculate the mass needed of $Fe(NO_3)_3$ and $Y(NO_3)_3$ using zero for $Bi(NO_3)_3$ and $Al(NO_3)_3$. YIG was produced via stock solution methodology using ethylene glycol as the solvent. This solution was heated in an alumina boat to form a powder and characterized using powder-XRD. Following successful YIG powder formation, films were again prepared with bismuth and aluminum doping on silicon with no magneto-optic response.

Dopants have been widely referenced for increasing the Faraday rotation of YIG films.[16] To date, most dopants have been rare earth lanthanides or p-block metals due to their increased magnetization and their ability to distort coordination environments

compared with the other elements. Bismuth, erbium, holmium and dysprosium were selected as likely candidates based upon their Verdet constants, relatively steady magnetization through likely application temperatures and atomic radius. There have been a number of papers published discussing the influence of bismuth substitution in yttrium iron garnet. These reports all display increased Faraday rotations of nearly twice that of yttrium iron garnets. [8,10,17,18,19] Bismuth was chosen due to this large increase in

Ion	Ionic radii (Å)	Lattice site preference in garnets ↓16*a*	↓24*c*	↑24*d*	Number of unpaired electrons[a]
Y^{3+}	0.95		1.0		0
Gd^{3+}	0.97		1.0		7
Yb^{3+}	0.93		1.0		1
Er^{3+}	0.97		1.0		3
Sm^{3+}	1.00		1.0		5
Dy^{3+}	0.92		1.0		5
Ho^{3+}	0.91		1.0		4
Tb^{3+}	0.93		1.0		6
Nd^{3+}	1.04		1.0		3
Bi^{3+}	0.93		1.0		0
Ca^{2+}	0.99		1.0		0
Fe^{3+}	0.66	0.4		0.6	5
Al^{3+}	0.51			1.0	0
Ga^{3+}	0.62			1.0	0
Cr^{3+}	0.64	1.0			3
V^{5+}	0.59			1.0	

[a] Based upon Harrison and Hodges (1972).

Figure 3-4 Ionic radii, lattice site preference in the garnet structure and unpaired electrons.[20]

Faraday rotation, however the ionic radius of bismuth is 0.93 Angstrom. The main difficulty associated with bismuth substitution was obtaining the preferred single crystal film because of material constraints: i.e. small number of garnet substrates with matching lattice parameters. Experimental evidence supports that these elements have the ability to produce large Faraday rotations while maintaining a relatively constant magnetization over a broader range of temperatures than the other elements selected.

Erbium was chosen because its ionic radius is 0.97 angstrom, as seen in Figure 3-4, which is slightly higher than the 0.95 angstrom radius for yttrium. It has an extremely high verdet constant as can be seen in Figure 3-5. The magnetization curve, Figure 3-6, is quite flat over the temperature range of interest (250-400 K) and erbium has the largest Bohr magneton response of all the proposed elements, approximately 5 in the temperature range to be examined. The only concern is its increased ionic radius with

respect to yttrium; this will again pose issues with respect to lattice matching and substrate selection. Methods to solve this involve the addition of a second, smaller element. Similarly to the aluminum doping in bismuth substituted YIG's.

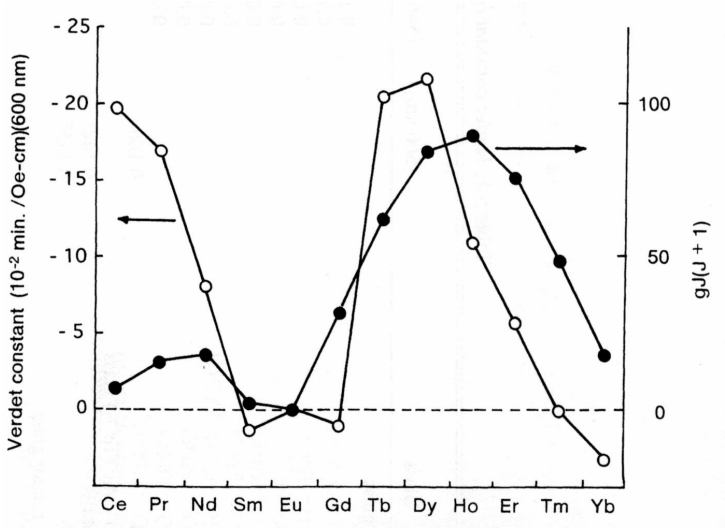

Figure 3-5 Verdet constant (λ=600nm) and n2eff/g for various trivalent rare-earth ions.[19]

Dysprosium, due to the fact that it has the same ionic radius as bismuth, should easily substitute for bismuth with respect to processing parameters for film formation. Its verdet constant, shown in Figure 3-5, is also above $5*10^{-2}$ min/Oe-cm. Although the magnetization curve is relatively low, approximately 3 Bohr magnetons, it is also relatively flat over the temperature range of 300-500K.

Despite the lack of a verdet constant, large atomic radius (0.97 angstroms) and loss of magnetization near room temperature dysprosium was the final candidate selected. The reason for choosing such a seemingly poor candidate was due to possible affinity of inducing a single crystal more readily on GGG due to the gadolinium attraction.

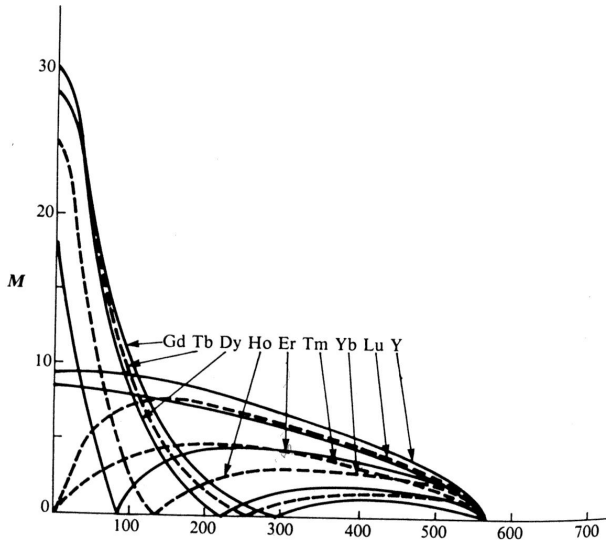

Figure 3-6 Magnetization curves for rare-earth iron garnets. Ordinate is Bohr magnetons, abscissa is temperature in Kelvin.[19]

Utilizing the same mixture calculations as for Bi,Al:YIG each candidate was substituted. Factoring in the hydration of the nitrate salts, Iterations #2 and 3 were utilized to back-calculate each metal nitrate mass required for obtaining the desired molecular formula, $R_2Y_1Fe_{4.6}Al_{0.4}O_{12}$. Experiments completed with the rare-earth dopants were limited to:

- Original mixing procedures using alternative rare-earth dopants substituted for bismuth
- stock solution methodology with ethylene glycol and ethyl aceto acetate as solvents

3.2.2 Deposition and Calcination

Substrate, deposition technique and calcination profiles were concurrently modified with mixing procedure to achieve a MO film. Alumina, glass slides, quartz, (110) silicon and (111) GGG were selected as substrate candidates. Solutions on alumina, glass slides and quartz were deposited only by spin coating. Spin coating, dip coating and a modified casting were used to deposit films on silicon and GGG. Alumina was the only substrate that displayed complete wetting of the sol-gel solutions. Unfortunately, at temperatures above 650°C the film pulverized into a powder. Glass slides had softened by 650°C and were therefore not pursued. Films on quartz, (110)

silicon and (111) GGG behaved similarly with respect to film cracking and wetting characteristics independent of deposition technique. However, high temperature film morphology differed. Figure 3-7a-c show optical microscopy pictures of Bi,Al:YIG films on GGG, quartz and silicon after calcination profile CP-1. Silicon was used in all experiments due to low cost and ease of integration as a substrate.

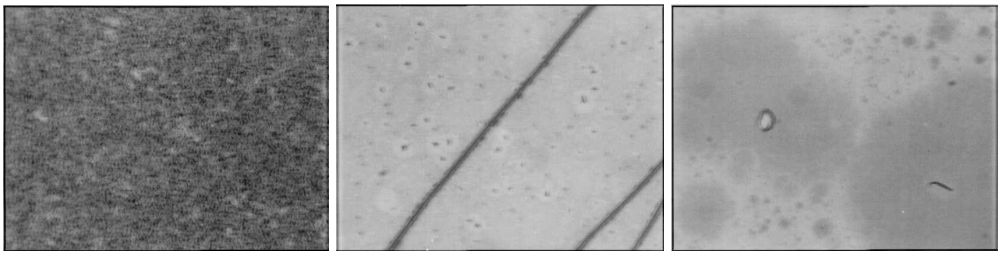

(a) (b) (c)

Figure 3-7 Bi,Al:YIG film cured at 700°C on GGG, quartz and silicon, respectively.

Surface pretreatments were examined by surface angle measurements due to the inability of solutions to wet silicon. Silicon was exposed to six wet chemical pretreatments and argon plasma cleaning. Using a 0.25M Bi,Al:YIG solution, none of the wet chemical treatments consistently increased wetting. In spite of improved solution wetting by plasma cleaning dewetting was not completely eradicated. Five wet chemical pretreatment techniques were evaluated by surface contact angle measurements, Table 3-2. The values listed indicate the polar and dispersive values of the silicon surface following the surface pretreatment technique. Despite changes in these values similar de-wetting characteristics of the sol-gel solutions were observed. This indicated that de-wetting arose primarily from the sol-gel solution incompatibility with the surface and an appropriate surfactant was required. Propionic acid was added to solutions as a surfactant for wetting substrates.[21] This aided in solution wetting, however more work was required with the concentration of propionic acid added because uniform wetting was not achieved.

Table 3-2 Surface contact angle measurements

Surface Pretreatment Technique	γ_p	γ_d
None	29.7	24.5
1	25.9	26.2
2	28.2	27.4
4	31.4	26.1
5	14.8	36.0
6	20.2	31.7
6[a]	7.7	33.9

[a] Si wafer in HF until etching was observed

Spin coating parameters, spin-on rpm/time and spin-off rpm/time, were optimized using silicon. Four techniques were examined with the values listed in Table 3-3:

1. Spin-on, pipette solution, spin-off
2. Pipette solution, spin-on, spin-off
3. Pipette solution, spin-off
4. Spin-off, pipette solution

Those shown in red are values associated with formulations in Table 3-1 that were utilized in the formation of films displaying a MO response. The most reliable technique was number four with a spin rate between 3500 and 4500 rpm and spin time approximately 120 seconds for a sol-gel solution of 0.25M as shown in Table 3-3. Solutions did not completely cover the substrates at lower spin rates and air bubbles were seen in films spun at higher rates. Due to variations in solution concentration and environmental effects a spin rate range is provided. Air movement and cleanliness also affected film wetting characteristics. Films developed in an environment with no air flow or a clean room with air flow wet a greater percentage of the substrate surface than a non-clean room environment with air flow.

Table 3-3 Spin coating parameters

ID	Spin-on (rpm)	Time (s)	Spin-off (rpm)	Time (s)
SC-1	500	10	2000	30
SC-1a	500	30	2000	60
SC-1b	500	45	2000	120
SC-2	500	10	2500	90
SC-3	500	10	3000	60
SC-4	500	10	4000	60
SC-5	500	10	5000	60
SC-6	1000	30	3000	30
SC-6a	1000	30	3000	60
SC-7	1000	10	3500	60
SC-8	1000	10	4000	30
SC-9	1000	10	5000	30
SC-10	1500	10	3500	60
SC-11	**1500**	**10**	**4500**	**120**
SC-12	1500	10	5500	120
SC-13	**None**	**None**	**4000**	**120**
SC-14	None	None	5000	120
SC-15	None	None	6000	120

Dip coating and a modified casting process were the other deposition techniques examined. Silicon and GGG substrates were dipped into a Bi,Al:YIG solution. Film quality was poorer than spin coated samples as the liquid gathered at the bottom of the substrate due to gravity. Only small areas near the bottom of the sample remained coated by the solution. Cracks were seen in all dip coated samples when subjected to any calcination profile. The modified casting process was developed for films greater than 1μm cured at 150°C. Both silicon and GGG were used with the modified casting process. A 0.25M Gd,Al:YIG solution was cast on both substrates, however only GGG based films showed MO response.

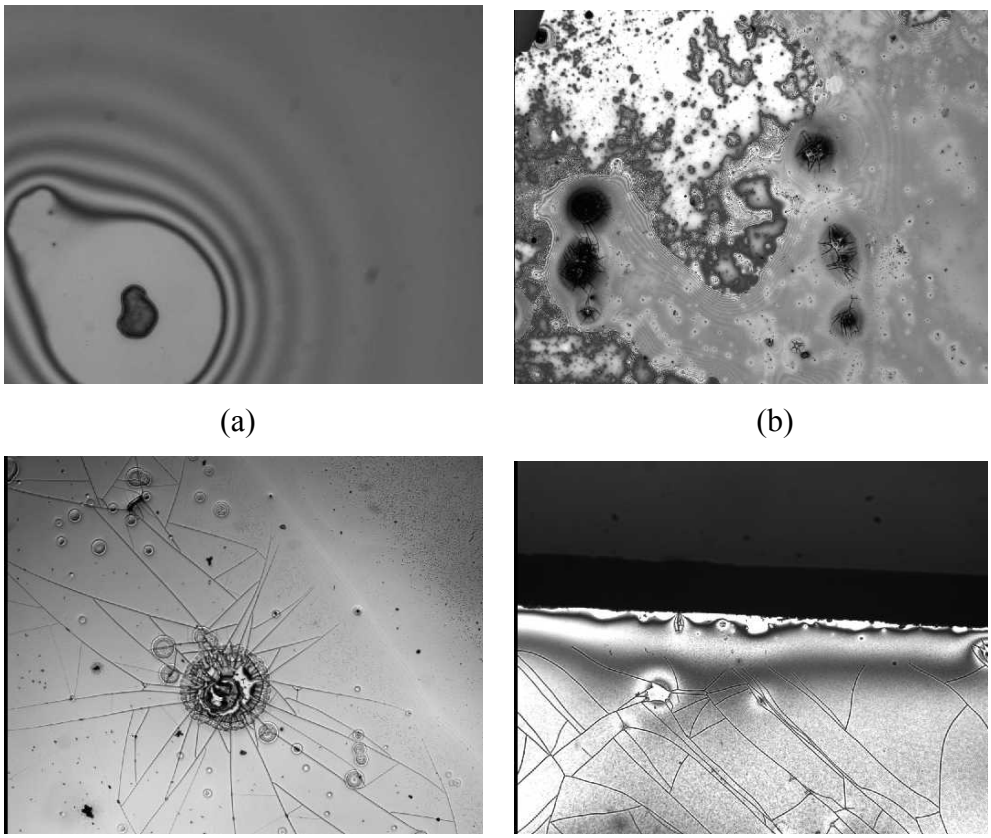

(a) (b)

(c) (d)

Figure 3-8 Bi,Al:YIG film cracking on silicon at 50, 110, 400 and 700°C, respectively.

To form a magneto-optical material it was important to exceed the Curie temperature to remove the natural magnetization of the elements. This is done to aid in crystallization and to align the magnetic domains with the intended orientation (perpendicular to the substrate surface) for easy axis magnetization. Calcination profiles were modified with respect to ramp rates, temperatures, steady state plateau times and atmosphere. Table 3-4, Table 3-5, Table 3-6 and Table 3-7 display the calcination profiles developed. The original calcination profile, CP-1, was intended for use with GGG as the substrate, therefore some processing issues (i.e. cracking, crystal formation) were expected to arise. Optical microscopy photographs of spin coated Bi,Al:YIG films, Figure 3-8a-d, display cracking with increasing temperature on silicon and modifications of the calcination profiles ensued. Reduction of crystallization temperature to 650°C to reduce film cracking while maintaining all other variables was the second attempted

calcination profile, CP-2. Both attempts utilized a slow ramp rate because of the expected stresses due to thermal expansion mismatches between silicon and the Bi,Al:YIG. CP-3 through CP-3d were implemented to identify low temperature processing parameters to improve film quality. The crystallization temperature was removed while maintaining the 50, 110 and 400°C steady state temperatures. Ramp rates and holding times were increased.

Table 3-4 Calcination profiles 1 – 7.

ID	T_1	R_1	t_1	T_2	R_2	t_2	T_3	R_3	t_3
CP-1	50	1	10	110	1	10	400	1	10
CP-2	50	1	10	110	1	10	400	1	10
CP-3	50	2	10	110	2	10	400	5	10
CP-3a	50	5	10	110	5	10	400	5	10
CP-3b	50	1	10	110	1	10	400	2	10
CP-3c	50	1	10	110	1	10	400	1	90
CP-3d	50	1	60	110	1	60	400	1	120
CP-4	50	1	10	110	1	10	400	2	10
CP-4a	50	1	10	110	1	10	400	2	10
CP-5	30	1	10	110	1	10	400	5	10
CP-6	80	1	120	110	1	120	400	1	120
CP-6a	80	1	120	110	1	120	400	1	120
CP-7	50	1	120	80	1	120	110	1	120

Table 3-5 Calcination profiles 1 – 7, continued.

ID	T_4	R_4	t_4	T_5	R_5	t_5	T_6	R_6	t_6
CP-1	700	1	240						
CP-2	650	1	240						
CP-3									
CP-3a									
CP-3b									
CP-3c									
CP-3d									
CP-4	700	10	240						
CP-4a	700	10	240						
CP-5	700	10	240						
CP-6	700	10	240						
CP-6a	700	5	240						
CP-7	400	1	120	700	10	240			

Following better results in film quality, the crystallization temperature of 700°C was reintroduced with modified ramp rates, CP-4. Allowing a film to stand for 24 hours before use of calcination profile CP-4 was conducted to reduce stress in the films. Further investigation to improve film quality was pursued by changing (CP-5 and CP-6) and adding low temperature steady state plateaus and ramp rates (CP-6a, CP-7). Removal of the steady state plateau below 100°C with further changes made in ramp rates and holding times were developed (CP-8, CP-8a, CP-8b). CP-9 and CP-10 utilized the original low steady state plateau temperatures while raising crystallization plateau temperatures to 725 and 750°C, respectively. Determination of the temperature at which cracking occurred was investigated by CP-11, a low temperature longer holding time calcination profile using low ramp rates. The combination of low temperature steady state plateaus in CP-11 with the crystallization steady state plateau of CP-1 was run in CP-12. The change in temperature from 190 to 225°C was enacted to dry the solvents, ethylene glycol and ethyl aceto acetate. Higher steady state crystallization temperatures were utilized with different ramp rates, low temperature steady state plateau temperatures and holding times.

Table 3-6 Calcination profiles 8 – 17.

ID	T_1	R_1	t_1	T_2	R_2	t_2	T_3	R_3	t_3
CP-8	110	1	120	400	1	120	700	1	120
CP-8a	110	2	120	400	2	120	700	10	120
CP-8b	110	5	60	400	5	120	700	5	240
CP-9	50	1	10	110	1	10	400	1	10
CP-10	50	1	10	110	1	10	400	1	10
CP-11	50	1	120	100	1	120	150	1	120
CP-12	50	1	120	100	1	120	150	1	120
CP-13	110	5	60	400	5	60	800	5	240
CP-14	50	5	70	110	1	70	400	1	120
CP-15	200	5	120						
CP-16	150	5	120						
CP-17	150	1	10	400	10	10	900	10	240

Table 3-7 Calcination profiles 8 – 17, continued.

ID	T_4	R_4	t_4	T_5	R_5	t_5	T_6	R_6	t_6
CP-8									
CP-8a									
CP-8b									
CP-9	725	10	240						
CP-10	750	10	240						
CP-11	190	1	240						
CP-12	225	1	240	400	5	120	700	1	300
CP-13									
CP-14	1000	5	360						
CP-15									
CP-16									
CP-17									

Powders were produced in both ambient and nitrogen atmospheres using CP-13 and CP-14. The resultant powders from CP-13 and CP-14 were characterized with powder-XRD. Due to successful crystal growth with powders, films on silicon were also made using calcination profiles CP-13 and CP-14 in both atmospheres. Cracking was more pronounced at the higher temperatures and silicon noticeably oxidized at 1000°C. Gd,Al:YIG thick films on GGG were developed and characterized by the MO loop tracer at low temperatures, calcination profiles CP-15 and CP-16 were used with the thick films. The final calcination profile, CP-17, was used to successfully produce MO Gd,Al:YIG films on GGG. Gd,Al:YIG films on silicon were also cured with CP-17, yet did not respond to characterization with the magneto-optical loop tracer.

3.2.3 Characterization

XRD provided invaluable guidance to developing high temperature MO responsive films. Data from YIG powders produced with calcination profiles CP-13 and CP-14 was collected with XRD and subsequently compared with literature crystalline structure for powder Bi,Al:YIG, shown in Figure 3-9. Clearly, the garnet crystal structure was forming at 800°C and nearly matched literature at 1000°C. The powders developed in an alumina boat were not exposed to a garnet crystal structure yet still developed the expected material. The logical conclusion from this data was that a film on

silicon and GGG would provide a MO response because of the ability to form a garnet crystal structure.

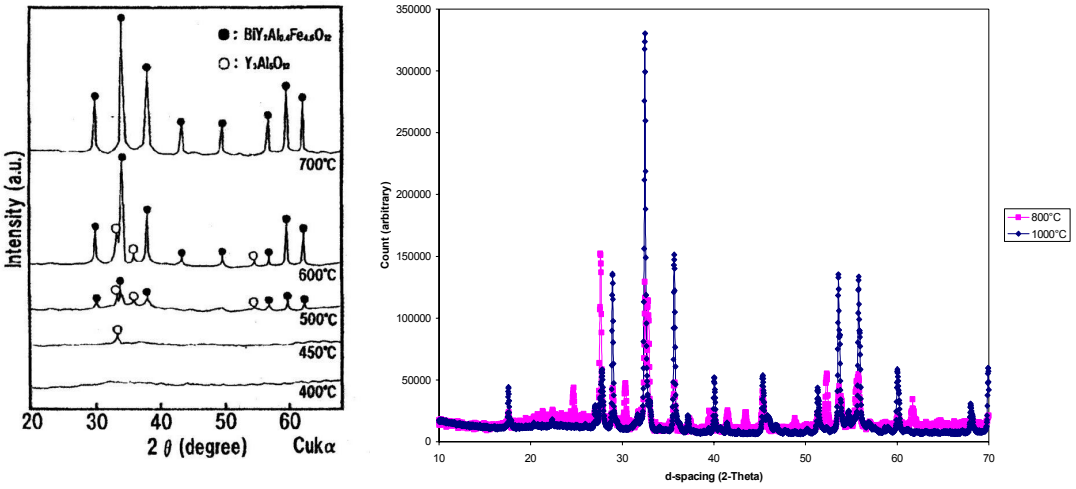

(a) (b)

Figure 3-9 (a) Literature Bi,Al:YIG powder. (b) Powder XRD of YIG formation at 800 (pink) and 1000°C (blue).

Thusly, Bi,Al:YIG films on silicon were produced via calcination profiles CP-13, CP-14 and characterized with a MO loop tracer. None of the films showed a response and therefore films on GGG were coated with both Bi,Al:YIG and Gd,Al:YIG. All films on GGG were characterized with the MO loop tracer at low and high temperatures. Gd,Al:YIG films on GGG using calcination profile CP-16 showed a response. This led to use of Gd,Al:YIG films processed with CP-17 and more films with MO responses. Table 3-8 displays the films that showed magneto-optic response, the magnitude of the response, objective film composition and final calcination/annealing temperature. Note that all films were deposited on (111) GGG. By definition a Faraday rotation was unable to be calculated because both signals either increased or decreased in strength. This cast doubt on the results, therefore the following calibration and improvements of the equipment ensued:

1. re-aligned laser beam to center of detectors
2. switched cables from detectors to lock-in amplifier
3. switched detectors
4. test with no sample in beam path

5. use of support for sample holder
6. use index matching gel

Table 3-8 Magneto-optical loop tracer data.

Film calculated composition	Film thickness[a]	Channel 1 (without magnet)	Channel 2 (without magnet)	Channel 1 (with magnet)	Channel 2 (with magnet)
Gd_2Y_1 $Al_{0.4}Fe_{4.6}O_{12}$ (150°C)	2.43 ± 0.94 μm	625 ± 5 nA	2.5 ± 0.05μA	537 ± 4 nA	2.160 ± 0.02 μA
Gd_2Y_1 $Al_{0.4}Fe_{4.6}O_{12}$ (150°C)	N/A	173 ± 6 nA	640 ± 12 nA	149 ± 5 nA	567 ± 9 nA
Gd_2Y_1 $Al_{0.4}Fe_{4.6}O_{12}$ (900°C)	1 ± 0.5 μm; peaks to 2μm	867 ± 5 nA	2.52 ± 0.05 μA	980 ± 7 nA	2.87 ± 0.07 μA
Bi_2Y_1 $Al_{0.4}Fe_{4.6}O_{12}$ (750°C)	167 ± 12 nm	1120 ± 30 nA	1.7 ± 0.04 μA	964 ± 25 nA	1.49 ± 0.03 μA
Gd_2Y_1 $Al_{0.4}Fe_{4.6}O_{12}$ (900°C)	158 ± 22 nm	986 ± 14 nA	1.4 ± 0.03 μA	862 ± 24 nA	1.22 ± 0.03 μA

[a] Film thickness determined by profilometry and ellipsometry.

Each of the above procedures was checked using the Bi,Al:YIG standard supplied by Airak, Inc. Each time the standard displayed the same behavior as the samples. The six techniques provided ample data proving that the samples did indeed show MO response. Additionally, the films did not show MO response over the entire surface area, which provided yet another data point that the signal intensity changes were not due to vibration or some other aberration. MO responsive films were subsequently investigated with SEM/EDS.

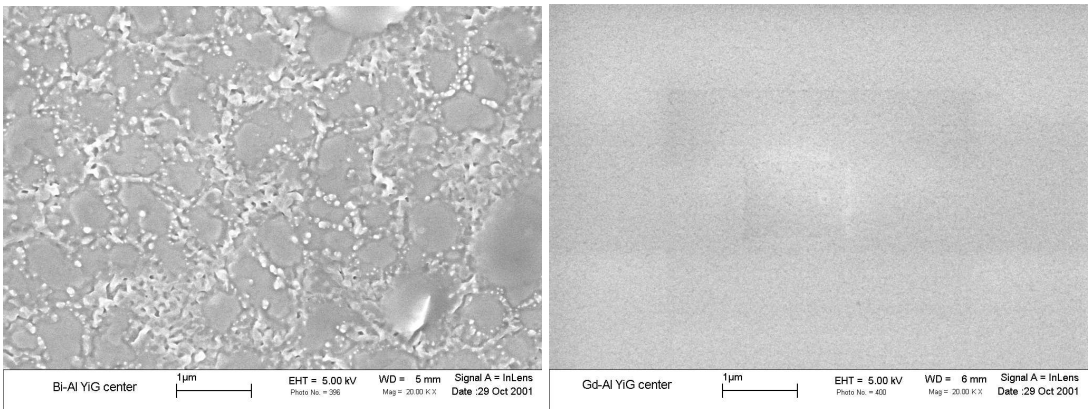

(a) (b)

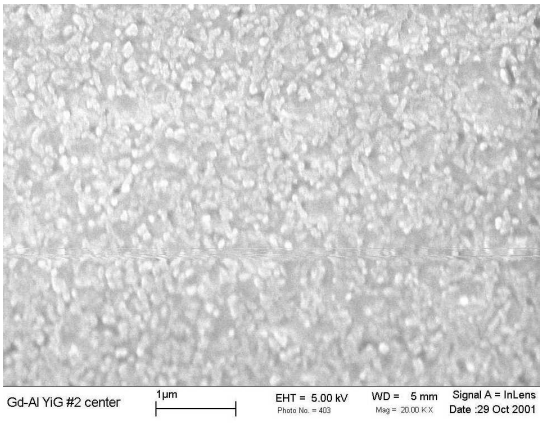

(c)

Figure 3-10 (a) SEM of 750°C Bi,Al:YIG film on GGG, (b) 150°C Gd,Al:YIG on GGG and (c) 900°C Gd,Al:YIG film on GGG at magnification of 20kX.

Low and high temperature (150 and 900°C, respectively) Gd,Al:YIG films with MO response were analyzed with SEM/EDS to view physical surface traits and elemental content. MO responsive Bi,Al:YIG films (750°C) were also evaluated. Figure 3-10a-c show the SEM photos taken at a magnification of 20kX. Shown are the morphological variations of these samples. A highly porous Bi,Al:YIG film can be seen which could be the result of non-epitaxial crystal growth and may account for why the film had only site specific MO properties. Gd,Al:YIG film displayed similar characteristics although the feature sizes are smaller and indicate a densification process. Conversely the Gd,Al:YIG amorphous films on GGG displayed virtually no surface variations and voids were not

seen due to solvent present. Once again the MO response was site specific, however the fact that a crystal was not grown and possible affinity of gadolinium in the film for gadolinium in the substrate may induce a MO response in a magnetic field. Table 3-9 shows the actual elemental composition, obtained via EDS, was always lower than the expected. Poor sol-gel reaction control and increased nitrate salt hydration easily explain lower elemental concentrations.

Table 3-9 Atomic percent elemental composition of $R_2Y_1Al_{0.4}Fe_{4.6}O_{12}$ films.

Film composition	R (rare-earth)	Y	Al	Fe	O
Expected R,Al:YIG	5.556	11.111	2.222	25.556	66.667
Actual Gd,Al:YIG	4.084	2.863	0.68	3.515	88.857
Actual Bi,Al:YIG	1.205	2.708	1.823	2.408	91.856

Ellipsometry and profilometry were used to determine film thickness of 0.125M solutions spin coated or cast following processing. Originally ellipsometry was used due to the versatility and accuracy of the characterization technique, especially with silicon as a substrate. All films characterized with ellipsometry were fitted using the Lorentz model. Ellipsometry is sensitive to all layers above the substrate and therefore the SiO_2 layer on silicon needed to be modeled for accurate determination of the R,Al:YIG film thickness. GGG had no oxide layer, which is reflected by N/A in Table 3-10 in the t_{SiO2} column. Another important factor in obtaining appropriate film thickness required a knowledgeable guess of the thickness without which local minima and maxima could adequately fit the data with unreasonable results, such as an oxide layer thicker than a film. Finally, the MSE column refers to the mean square error of the model with respect to the collected data. An accurate fit is indicated by a MSE value closer to zero. An interesting observation of silicon based films was that modeling rarely provided a total film thickness above 100nm when adding the oxide layer with the film thickness. Profilometry was also used because samples were unable to be accurately modeled on GGG, could not fit the sample holder of the ellipsometer and film uniformity and wetting were unacceptable to be modeled without MSE's almost double those on silicon. Film dewetting actually proved useful for implementation of profilometry because a flat surface was required for obtaining a film thickness. Shown is the average film thickness

and error obtained by profilometry. Only one low temperature film thickness was measured because films were still tacky and the stylus was fouled.

Table 3-10 Film thickness of $R_2Y_1Fe_{4.6}Al_{0.4}O_{12}$ films.

Technique	Substrate	Film Composition	t_{film} (nm)	t_{SiO2} (nm)	MSE
Ellipsometry	Si	$Bi_2Y_1Fe_{4.6}Al_{0.4}O_{12}$	103.8±3.9	0±3.8	29.52
Ellipsometry	Si	$Bi_2Y_1Fe_{4.6}Al_{0.4}O_{12}$	112.3±3.2	0±3.3	27.61
Ellipsometry	Si	$Bi_2Y_1Fe_{4.6}Al_{0.4}O_{12}$	65.0±2.7	28.9±2.5	25.61
Ellipsometry	Si	$Bi_2Y_1Fe_{4.6}Al_{0.4}O_{12}$	59.5±3.3	41.61±3.0	27.46
Ellipsometry	Si	$Bi_2Y_1Fe_{4.6}Al_{0.4}O_{12}$	21.8±1.2	98.0±1.3	47.47
Ellipsometry	GGG	$Gd_2Y_1Fe_{4.6}Al_{0.4}O_{12}$	158.1±12.2	N/A	61.06
Ellipsometry	GGG	$Bi_2Y_1Fe_{4.6}Al_{0.4}O_{12}$	167.8±22.8	N/A	61.37
Profilometry	GGG	$Gd_2Y_1Fe_{4.6}Al_{0.4}O_{12}$	1000±500	N/A	N/A
Profilometry	GGG	$Gd_2Y_1Fe_{4.6}Al_{0.4}O_{12}$	2430±940	N/A	N/A

CHAPTER 4 Conclusions and Recommendations

The goal of the thesis was the development of $R_xY_{3-x}Al_yFe_{5-y}O_{12}$ films. Significant findings are listed below:

1. XRD verified sol-gel processing parameters utilized in the formation and growth of $R_xY_{3-x}Al_yFe_{5-y}O_{12}$ crystal structure at 800 and 1000°C, respectively.
2. Mixing procedure changes eliminated sol-gel solution explosive reactions.
3. Change in surface morphology with temperature was shown via SEM.
4. EDS verified Y, Al, Fe, O and R present in the films.
5. Crystalline Bi,Al:YIG, Gd,Al:YIG and amorphous Gd,Al:YIG films with compositions $Gd_2Y_1Al_{0.4}Fe_{4.6}O_{12}$ and $Bi_2Y_1Al_{0.4}Fe_{4.6}O_{12}$ displayed MO behavior.

In conclusion, it has been shown that sol-gel formulation, deposition, and calcination profile development led to garnet crystal structure formation and growth as verified by XRD. Change in surface morphology as a function of temperature was shown by SEM micrographs and EDS verified the expected elements in the films. Addition of propionic acid appeared to reduce the percentage of dewetting on silicon and GGG, but the ability to eliminate film cracking was never achieved. Use of ethyl aceto acetate in addition to development of stock solution methodology eradicated uncontrolled exothermic reactions. Finally, $Gd_2Y_1Al_{0.4}Fe_{4.6}O_{12}$ and $Bi_2Y_1Al_{0.4}Fe_{4.6}O_{12}$ films displayed MO behavior in accordance with a Bi,Al:YIG standard.

Recommendations include gaining a more rigorous understanding of the sol-gel chemistry with respect to the metal nitrate chemistry viewpoint for future advances. This can be attained through electron probe microanalysis (EPMA) and x-ray photo spectrosocopy (XPS) by evaluating elemental composition of films and solutions as compared with expected. Additionally, use of liquid and solid state NMR to identify phases and coordination states of gels and films is of utmost importance to gaining the understanding and knowledge of the reactions and products formed. Silica sol-gel processing requires a surfactant for deposition and YIG sol-gel displays similar requirements as displayed by inconsistent wetting characteristics. Investigation of propionic acid as a surfactant is suggested. XRD of YIG films on GGG to determine

viability and highest calcination temperature needed, respectively. The low temperature film is of further interest and would prove very useful as an integrated sensor due to the 150°C processing temperature well within electronics industry processing temperatures.

These suggestions match well with a conclusion stated by J.Livage, et al., "A real mastery of the sol-gel process is required from both scientific knowledge and technological expertise point of view…Many parameters are involved along the process: chemistry during hydrolysis and condensation of the precursors, physical chemistry of aggregation, gelation, drying and finally physics to account for the properties of materials. Each step has to be optimized depending on the required application. More reliable experimental data and accurate characterization of all the chemical species involved in the reactions have to be obtained before a real science of inorganic polymerization can be established."[22]

REFERENCES

[1] "Fibre Optic Magnetic Field Sensors Using Iron Garnet Materials" PhD Thesis by Hans Sohlström, 1993

[2] M. J. Caruso, T. Bratland, C.H. Smith, R. Schneider, "A New Perspective on Magnetic Field Sensing," www.ssec.honeywell.com, (1998)

[3] N. Inoue, K. Yamasawa, "Stabilization of Temperature Dependence of Verdet Constant of Bi-Doped Garnet and Development of High Sensitive Optical Fiber Magnetic Field Sensor," *Elect. Eng. In Jpn.,* **117** [1], 1 (1996)

[4] Guofeng Bai, Personal conversation

[5] K. Matsuda, S. Ishizuka, "Three-dimensional $(BiY)_3Fe_5O_{12}$ waveguide with a load layer made of SiO_2", Applied Optics, **30** [15], (1991)

[6] E. Kato, T. Sei, T. Tsuchiya, "Preparation of highly oriented thin film exhibiting a magneto-optic effect in Bi, Al doped YIG," *J. Cer. Soc. Jpn.,* **102** [9], 818 (1994)

[7] M. Inoue, T. Nishikawa, H. Otsu, H. Kominami, T. Inui, "Synthesis of rare-earth gallium garnets by the glycothermal method," *J. Am. Ceram. Soc.,* **81** [5], 1173 (1998)

[8] T. Tsuchiya, T. Sei, H. Kanda, "Sol-gel preparation of YIG thin film showing opto-magnetic effect," *J. Non-Cryst. Solids,* **147**&**148**, 463 (1992)

[9] L.L. Hench, J.K. West, *"Principles of Electronic Ceramics"*, John Wiley & Sons, New York, 1990

[10] K. Matsumoto, S. Sasaki, Y. Yamanobe, K. Yamaguchi, T. Fujii, Y. Asahara, "Bismuth and aluminum substituted YIG single crystal films on modified gadolinium gallium garnet single crystal substrates," *J. Appl. Phys.,* **70** [3], 1624 (1991)

[11] K. Matsumoto, S. Sasaki, K. Yamaguchi, T. Fujii, Y. Asahara, "Highly bismuth substituted yttrium iron garnet single crystal films prepared by sol-gel method," *J. Magn. Mag. Matls.,* **104-107**, 451 (1992)

[12] Jeffrey C. Brinker, *"Sol-Gel Science: The Physics and Chemistry of Sol-Gel Processing"*, Academic Press, Inc., San Diego, 1990

[13] R.W. Jones, "*Fundamentals of Sol-Gel Technology,"* The Institute of Metals 1998

[14] B.J.H. Stadler, K. Vaccaro, A. Davis, G.O. Ramseyer, E.A. Martin, H.M. Dauplaise, L.M. Theodore, and J.P. Lorenzo, "Optoelectronic Properties of Transition Metal and Rare Earth Doped Epitaxial Layers on InP for Magneto-Optics," *J. Electronic Matls.,* **25** [4], 709 (1996)

[15]Peter A.S. Smith, *"The chemistry of open-chain organic nitrogen compounds"*, W.A. Benjamin, Inc., 1966

[16] E.P. Wohlfarth, "*Ferromagnetic Materials Vol. 2*," North Holland Publishing Co., New York, 1980

[17] K. Matsumoto, K. Yamaguchi, and T. Fujii, "Preparation of bismuth-substituted yttrium iron garnet powders by the citrate gel process," *J. Appl. Phys.*. **69** [8], 5918 (1991)

[18] T. Okuda, T. Katayama, K. Satoh, and H. Yamamoto, Preparation of polycrystalline $Bi_3Fe_5O_{12}$ garnet films, J. Appl. Phys **69** [8], 4580 (1991)

[19] M-Y Chern and J-S Liaw, "Study of $Bi_xY_{3-x}Fe_5O_{12}$ thin films grown by pulsed laser deposition," *Jpn. J. Appl. Phys.*, **36** [1:3A], 1049 (1997)

[20] M. Yamane, Y Asahara, *"Glasses for Photonics,"* Cambridge University Press, New York, 2000

[21] X. Ma, S. Zhang, F. Li, D. Que, "Preparation of bismuth substituted dysprosium iron garnet film by a sol-gel process", *J. Matls. Sci.:Matls. in Electronics,* **9,** 347 (1998)

[22] J. Livage, M. Henry, C. Sanchez, "Sol-gel chemistry of transition metal oxides", *Prog. Solid St. Chem.,* **18,** 259 (1988)